Sensors & Actuators: B. Chemical 381 (2023) 133395

Contents lists available at ScienceDirect

Sensors and Actuators: B. Chemical

journal homepage: www.elsevier.com/locate/snb

Rapid and reversible detection of trace amounts of H_2S in air and packaged food using a biogenic bismuth oxide nanorod colorimetric sensor

Monica Jaiswal [a], Robin Kumar [a,*], Ravi Mani Tripathi [a], Ranu Nayak [a], Jagjiwan Mittal [a], Sumit Choudhary [b], Satinder K. Sharma [b]

[a] Amity Institute of Nanotechnology, Amity University, 201303 Uttar Pradesh, India
[b] Indian Institute of Technology, Mandi, HP, India

ARTICLE INFO

Keywords:
H_2S gas
Bismuth Oxide
Reversible sensor
Meat packaging
Colorimetric sensor

ABSTRACT

A colorimetric reversible sensor has been developed for detection of trace amount of H_2S gas in air and sealed meat packages. The active sensing area includes high surface area bismuth oxide (Bi_2O_3) nanorod prepared by green synthesis method. The as fabricated sensor demonstrates a rapid response in just 25 s for sensing 1 ppm H_2S gas with distinct colour change in the active sensing area from white to brown. Sensing pellets were used to optimize the performance of the H_2S sensor in terms of sensitivity and selectivity in air. Flexible nitrocellulose membrane filter papers coated with Bi_2O_3 were used to detect spoilage in packaged raw animal food products such as meat, poultry and fish. The sensor is reversible and can be recovered within a short cycle (3 min) of heat treatment at 300 °C. X-ray diffraction, Raman spectroscopy and band gap measurements confirmed partial conversion of Bi_2O_3 nanorods into Bi_2S_3 when exposed in the range of 1–100 ppm H_2S gas.

1. Introduction

Hydrogen sulphide (H_2S) is one of the most dangerous gases present in our environment. Exposure to low H_2S concentration can lead to many critical health problems such as eye and throat injury, poor memory, dizziness, and loss of sense of reasoning and balance. At concentrations of 100 parts per million (ppm) or more, H_2S can immediately lead to death [1]. Apart to human bodies, sulphur compounds can also corrode metallic equipment and poison catalysts, resulting in economic losses. Additionally, sulphur compounds in fuel gases will be oxidized to SO_2, causing air pollution and health problems [2,3]. Emission sources are majorly petroleum/natural gas drilling and refining, coke ovens, tanneries, landfills, sewage plants, kraft mills, asphalt plants and natural gas industries etc.[4]. According to Occupational Safety and Health Administration (OSHA) the permissible exposure limit of H_2S gas in air is 10 ppm for 8-hour work shift [5]. Numerous materials including semiconductor metal oxide, conductive polymers, quantum dots, nanocomposites with carbon nanotubes (CNT) have been explored and studied for sensing H_2S gas to lowest concentration possible [6,7].

Many techniques have been explored to detect the presence of H_2S gas, including conductivity impedance, potentiometry, amperometry, colorimetry, absorption, fluorescence etc.[8]. Visual detection of H_2S using Colorimetric probes have drawn considerable attention due to various advantages such as rapid sensing, facile detection with the naked eye, and low-cost measurements [9]. Other than easy detection of H_2S gas in air using colorimetric sensor, its application in smart food packaging is also a convenient solution in identifying spoilage of food. During meat storage, decomposition of sulfur-containing amino acids takes place due to enzymatic hydrolysis of bacteria, which produces a series of mercaptans, which eventually decompose into H_2S. Hence, H_2S is considered as an indicator to assess meat spoilage [10,11]. In recent years, various advanced colorimetric sensors for H_2S are reported that includes use of ruthenium nanoparticles (Ru NPs) [12], silver and polymer composites [13], polyaniline coated fabric [14], copper and lead acetates [15,16], functionalized gold and silver nanoparticles [11, 17], etc. These sensors have demonstrated high selectivity and sensitivity towards detection of H_2S typically during food spoilage. A Bismuth derivative based colorimetric sensor for H_2S gas was explored where alkaline bismuth hydroxide ($Bi(OH)_3$) could sense H_2S gas as low as 30 ppb at room temperature [18]. In spite of excellent sensitivity, the sensor was limited to one-time use being irreversible in nature. Another derivative of bismuth, α-$Bi_2Mo_3O_{12}$ shows change in colour in H_2S gas, forming stable sulfides [19]. Surprisingly, reversibility of colorimetric H_2S gas sensor is barely studied. To reduce the cost of sensor,

* Corresponding author.
E-mail address: rkumar5@amity.edu (R. Kumar).

https://doi.org/10.1016/j.snb.2023.133395
Received 17 September 2022; Received in revised form 13 January 2023; Accepted 18 January 2023
Available online 23 January 2023

reversibility and hence reusability of gas sensors is one of the major properties.

In view of developing a simple, low-cost and highly sensitive H_2S sensor, in the present work, we have fabricated a bismuth oxide nanorod for detection of trace levels H_2S gas. Bismuth oxide is an important metal oxide semiconductor which has been receiving considerable attention because it exhibits excellent optical and electrical properties such as wide bandgap, high refractive index, high dielectric permittivity and good photoconductivity [20]. Due to these properties, it has found many applications including gas sensors. Bismuth based various nanostructures and nanocomposites are often studied for gas sensing [21–26]. The bismuth oxide sensing material has been synthesized biogenically as high aspect ratio, high surface area nanorods that assists to achieve a high sensitivity. The as fabricated semi quantitative colorimetric H_2S sensor can detect trace amounts of H_2S in air as low as 310 ppb. In addition, the sensor has been successfully tested for detecting spoilage in packaged raw animal products, such as meat, poultry and fish.

2. Materials and methods

2.1. Materials

Ficus benghalensis's fresh leaves were collected from Amity University campus, India. Glacial acetic acid, sodium hydroxide and bismuth nitrate pentahydrate were procured commercially from Merck.

2.2. Synthesis

Fresh leaves of *Ficus benghalensis* (25 gm) were chopped and dispersed in 150 ml deionized water (DI), followed by stirring (450 rpm) at 100 °C for 2 h. Thereafter, the solution was filtered, and an extract was obtained (solution A). Solution B was prepared by mixing bismuth nitrate pentahydrate (0.95 M) with 5 ml glacial acetic acid and was stirred at 60 °C to obtain clear solution. This solution was then mixed with 4 ml of solution A and further diluted with 25 ml DI water. The mixture was then added with 30 ml 0.24 M sodium hydroxide solution drop wise and continued the reaction for 1 hr under stirring condition at 60 ℃. The resultant solution turned into pale yellow precipitate of Bi_2O_3. The precipitate was separated by centrifugation and dried at 80 °C to obtain bismuth oxide nanorods [27]. The leaf extract of *Ficus benghalensis* has high amount of flavonoid which acts as a reducing agent to synthesize nanorods. The leaf extract also provide stability to the nanorods by encapsulating with the protein present in the leaf extract. The reproducibility can get affected if plant species will change. It will not change if closely related species like *Ficus panda* is used for leaf extract preparation. Hence, the reproducibility of nanorods will not be influenced if *Ficus benghalensis* of any origin take in the synthesis with analogous parameters.

2.3. Characterization tools

Scanning electron microscopy (SEM) and Energy dispersive X-ray spectroscopy (EDX) was done on powdered form of sensor material to study the surface morphology and elemental composition of the synthesized nanomaterial. X-Ray diffraction (XRD) with CuKα, $\lambda = 1.54$ Ǻ was used to study the crystalline structure of synthesized sensing material. Raman spectroscopy using Horiba Jobin Yvan Labram HR with 532 nm and 3 mW laser was used to determine the composition of sensor material. UV-Visible spectroscopy was performed between 400 and 800 nm on a pellet of sensor material to study the effect of gas on the optical properties of the H_2S exposed material. Surface area of sensor material was studied using Brunauer-Emmett-Teller (BET) on Quanta chrome Model Autosorb iQ3.

3. Experimental

3.1. Fabrication of sensor

Sensor element was prepared in three forms, a) powder form, b) pellet form, c) coated on flexible substrate. A ceramic plate of (2 cm × 1 cm) with a hemispherical cavity (diameter 0.2 cm and surface area of 0.031 cm^2) was used as sensor element. Powder of nanorods of bismuth oxide were press filled in the cavity to make the sensor element as shown in Fig. 1(a). Sensor material (Bi_2O_3 nanorods) was pressed by 1.5 ton weight using KBR pellet machine to form pellet of 1 cm diameter and thickness of 0.5 mm. As prepared pellet was used to study the light absorbance of material using UV-Vis spectroscopy, as shown in Fig. 1(b). For flexible sensor, sensor material was coated on flexible substrates like paper or fabric, Fig. 1(c).

3.2. Gas sensing method in air

Sensor element was kept inside gas sensing chamber, as shown in Fig. S1 of supplementary material. Glass lid present on the top of the sensing chamber was used to observe the transformation in the colour of sensor with the change in environment. The sample placed in the evacuated chamber was exposed with known concentration of H_2S gas (26 ℃) and images of the sensor were captured for multiple cycles. The recovery of the sensor was done by heating the sensor element at 300 ℃ in air.

3.3. Gas sensing method in raw animal food packaging

Fresh chicken, pork and fish samples were purchased from local market and transported to the lab in clean and cold environment (4 ℃). Pork was cut into 10 pieces of 10 gm each, and kept in closed vessel having sensor element at room temperature (27–30 ℃) for 6 days. The vessel humidity was measured as 30% RH. Similarly, fish and chicken were cut into pieces of 10 gm each. Fish pieces were kept in similar vessel with sensor at 4 ℃ for 6 days. On the other hand, pieces of chicken were saved at both 26 ℃ and 4 ℃ temperatures for 6 days. To observe the change in sensor colour images of all the samples were captured each day after every 24 h.

3.4. Data analysis and quantification

Sensor data was collected for multiple consecutive cycles of H_2S gas exposure by using UV-Vis spectroscopy and by recording the change in red green and blue (RGB) colours values of sensor element. Absorbance of sensor material was studied before and after exposure of H_2S gas, using Shimadzu UV-2600 plus. In order to measure RGB values change, photographs of sensor sample were taken before and after controlled exposure of H_2S gas using mobile camera (Samsung galaxy M21) from a distance of 15 cm in same conditions each time. The captured images were cropped into 1 × 1 cm^2 areas. For quantitative evaluation of colour change in sensor, the mean RGB values of the cropped images were extracted using Image J, (shown in Fig.S2 in supplementary file) which is an image processing program. Using difference in RGB values of

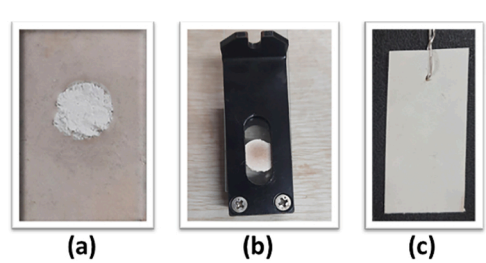

Fig. 1. Bi_2O_3 nanorods (a) in powder form on ceramic plate (b) compressed pellet (c) coated on fabric.

before and after exposure of H_2S gas, ΔR, ΔG, ΔB values were calculated. In Commission Internationale de l'Eclairage Lab (CIE L* a* b*) system, RGB values can be converted into L* a* and b* , representing lightness, red/green, and yellow/blue, respectively[28,29]. After conversion of values, change in the colour of sample (ΔE) was calculated using formula,

$\Delta E = \{(\Delta L^*)^2 + (\Delta a^*)^2 + (b^*)^2\}^{1/2}$ [30].

Change in colour (ΔE) greater than 3.3 is reported to be clinically accepted as it is identifiable with naked human eyes [15].

4. Results and discussion

4.1. Characterisations of sensing material

Fig. 2(a) shows the SEM micrograph of pristine bismuth oxide nanorods [32]. The micrographs depicted a range of lengths of the nanorods ranging from 2 to 100 μm with 388 nm as the average diameter. Elemental analysis of nanorods by EDX shows (Fig. 2b) the presence of bismuth and oxygen which indicate the presence of an oxide of bismuth in nanorods. A photograph of nanoroads power in Fig. 2(c) shows its white colour similar to Bi_2O_3.

X-ray diffraction studies in Fig. 2(d) shows the various peaks of bismuth compound. When compared using JSPDS card, these peaks belong to Bi_2O_3 [31,32] This compound has monoclinic crystal structure and pseudo-octahedral geometry. Miller indices of all the peaks are provided in the figure. Raman spectrum of Bi_2O_3 in Fig. 2(e) nanorods demonstrates peaks at 157, 109, 205, 325, 427, 512, 589 cm^{-1}. This is similar to the Raman spectrum of Bi_2O_3 in earlier studies [33–35].

4.2. H_2S gas sensing in air

Change in morphology of sensor material after exposure to 50 ppm H_2S gas was studied by SEM. Micrograph in Fig. 3(a) shows rod-like structure similar to unexposed material. However, some additional tiny fibrous structures are visible along the walls of the nanorods. Elemental analysis using EDX shows the presence of 1.6% atomic sulphur (Fig. 3(b)) in the material. Low amount of sulphur in materials demonstrates the conversion of small amount of Bi_2O_3 into Bi_2S_3 on exposure of H_2S gas. On exposure with 50 ppm H_2S gas at 26 ℃, the sensing material changed its colour distinctly from white to brown within 60 s, as shown in (Fig. 3c).

X-ray diffraction study of H_2S exposed sample in (Fig. 3(d)) shows the presence of few extra peaks in addition to Bi_2O_3 peaks. These peaks are due to Bi_2S_3 peaks as the positions and relative intensities of all the peaks are in good conformity with the orthorhombic crystal structure of Bi_2S_3 indexed in JCPDS card number 17–0320 as (220), (310) (211), (221) [36]. However, as seen in the Fig. 3(d), most of the material is Bi_2O_3. Raman spectrum of nanorods in Fig. 3(e), after exposure to H_2S gas displays peaks at 140, 200, 325 and 478 cm^{-1}. The peaks at 200 and 325 cm^{-1} indicates the presence of oxide and other two peaks 140 and 478 cm^{-1} shows the formation of Bi_2S_3 [37,38] due to exposure of H_2S gas.

4.3. Recovery optimization

Recovery efficacy was studied by keeping the sensor at 26 ℃ in a H_2S gas free environment for 24 h. However, no recovery was observed visibly, as the brown colour of the sensing material remained unchanged. Thereafter, the sensor material was heated at higher temperatures from 200 °C to 300 °C in air. Images were recorded and shown in Fig. 4(a), at different temperatures of annealing with an interval of 20 °C with respect to time of 60 s interval. Visual observation shows that the sample was not recovered between 200 and 240 °C even after heating up to 3 min. In fact, colour of exposed material was not changed to white at 200 °C even after heating for 1 hr. A visible recovery was observed after heating at 300 °C for 3 min, when the colour of sensor changed to original white from brown. Change in absorbance of pellet pre-exposure, post-exposure and after recovery at 500 nm wavelength were recorded. Absorbance spectra of sensor material supports the experimental observation of complete recovery at 300 °C, as shown in Fig. 4(b). Absorbance before and after heating H_2S gas exposed sample almost coincides.

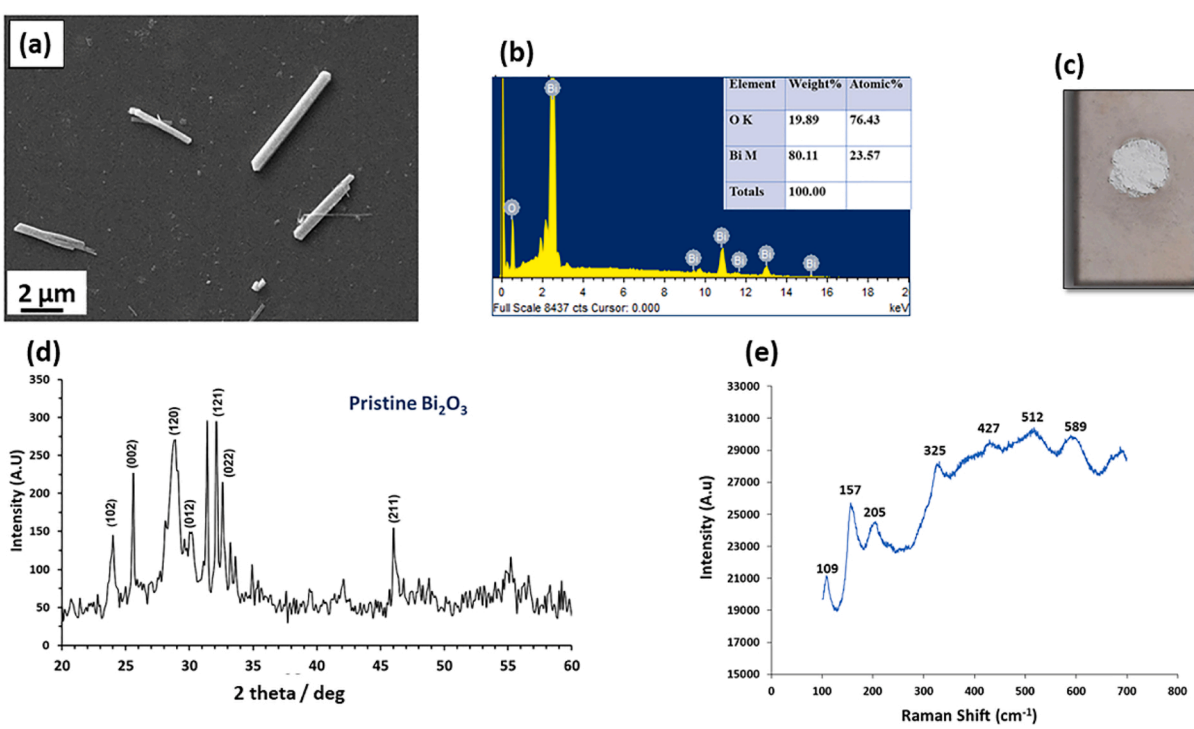

Fig. 2. (a) SEM images of pristine Bi_2O_3 nanorods (Image taken from [32] with permission of Taylor and Francis (b) EDX of nanorods shown in (a), (c) photograph showing bismuth oxide nanorods in powder form (d) XRD pattern and (e) Raman spectrum of Bi_2O_3 nanorods.

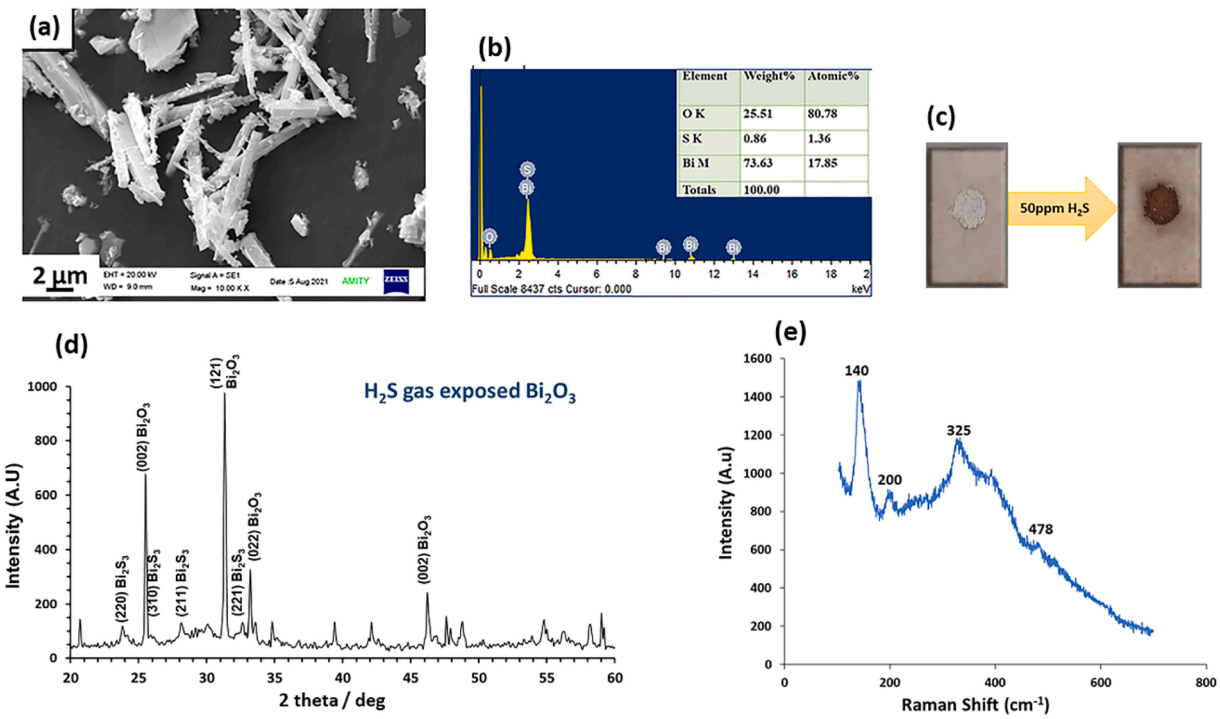

Fig. 3. (a) SEM micrograph showing Bi_2O_3 nanorods after exposure to 50 ppm H_2S gas (b) EDX analysis of nanorods in (a), (c) Change in colour, (d) XRD pattern and (e) Raman spectra of the of exposed Bi_2O_3 of Bi_2O_3 pallets after treatment with H_2S.

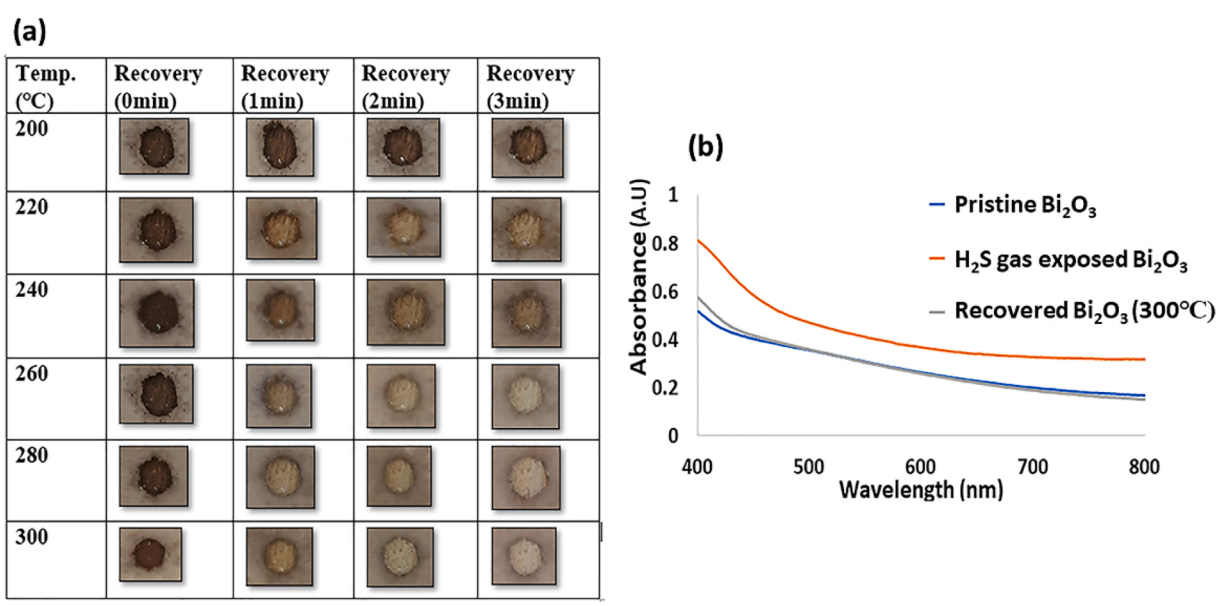

Fig. 4. (a) Recovery optimization from 200 to 300 ℃ (b) UV-Vis absorbance spectra after recovery.

Structure and elemental composition of recovered sensor material was studied and presented in Fig. 5. SEM micrograph in the 5(a) shows that the original nanorod structure of the sensor material is recovered with very few fibrous structures along its wall. Elemental analysis of the recovered material by EDX spectrum shows only the presence of bismuth and oxygen (Fig. 5(b)) in the material. Colour changed back to white as observed from naked eyes, shown in Fig. 5(c). This shows that the materials fully converted again to Bi_2O_3. X-ray diffraction study of recovered sample in (Fig. 5(d)) also showed the peaks due to Bi_2O_3 only. Raman spectrum of recovered nanorods in Fig. 5(e) displays peaks at 160, 200, 325, 512 and 589 cm^{-1}, similar to pristine Bi_2O_3 nanorods suggests that on heating exposed sensor material at 300 °C converts back to initial state.

4.4. Reversibility and repeatability

Fig. 6(a) shows repeatability of sensor, detection of H_2S gas in images. Sensor reversibility and repeatability was studied for 20 continuous cycles using UV-Visible spectroscopy after exposing a sensor pellet to 5 ppm of H_2S gas at 26 ℃ and subsequent recovery by heating for 3 min at 300 ℃. Out of 20 cycles, results of ten are shown in Fig. 6(b), further details of the study are provided in supplementary file (Fig.S3).

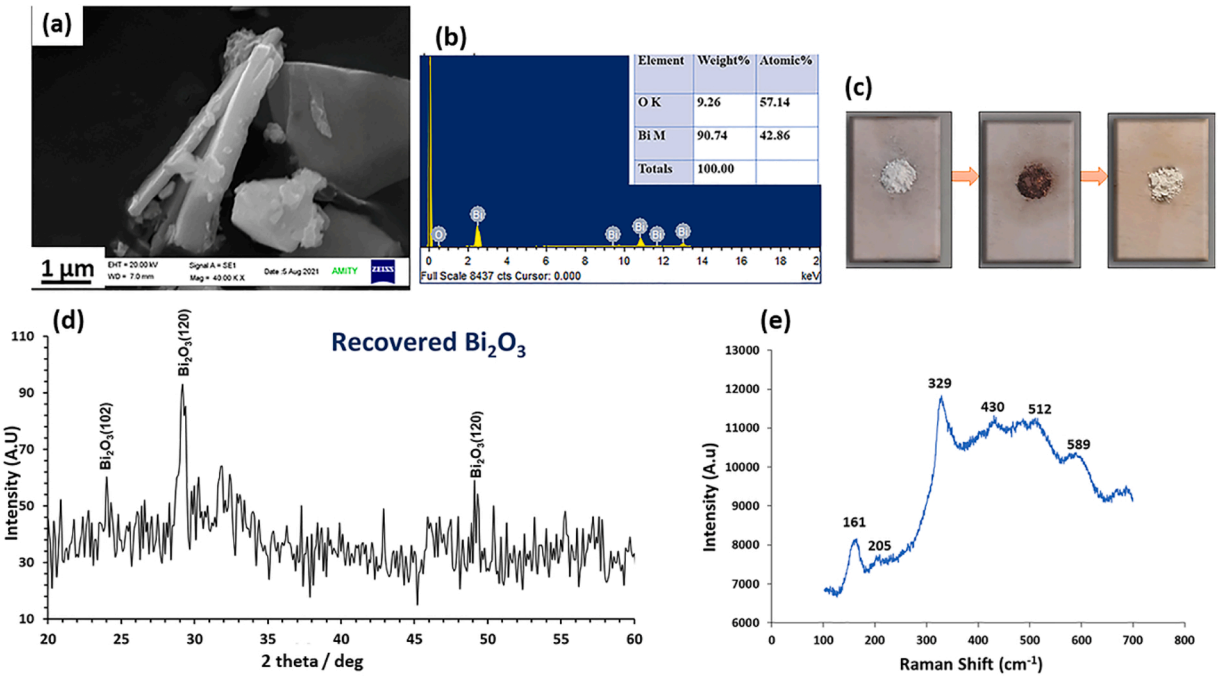

Fig. 5. (a) SEM micrograph of recovered Bi_2O_3 nanorods from after heating 5 ppm H_2S gas exposed Bi_2O_3 at 300 °C (b) EDX analysis of nanorods (c) Change in colour of Bi_2O_3 pallets during exposure and recovery (d) XRD pattern and (e) Raman spectra of recovered Bi_2O_3.

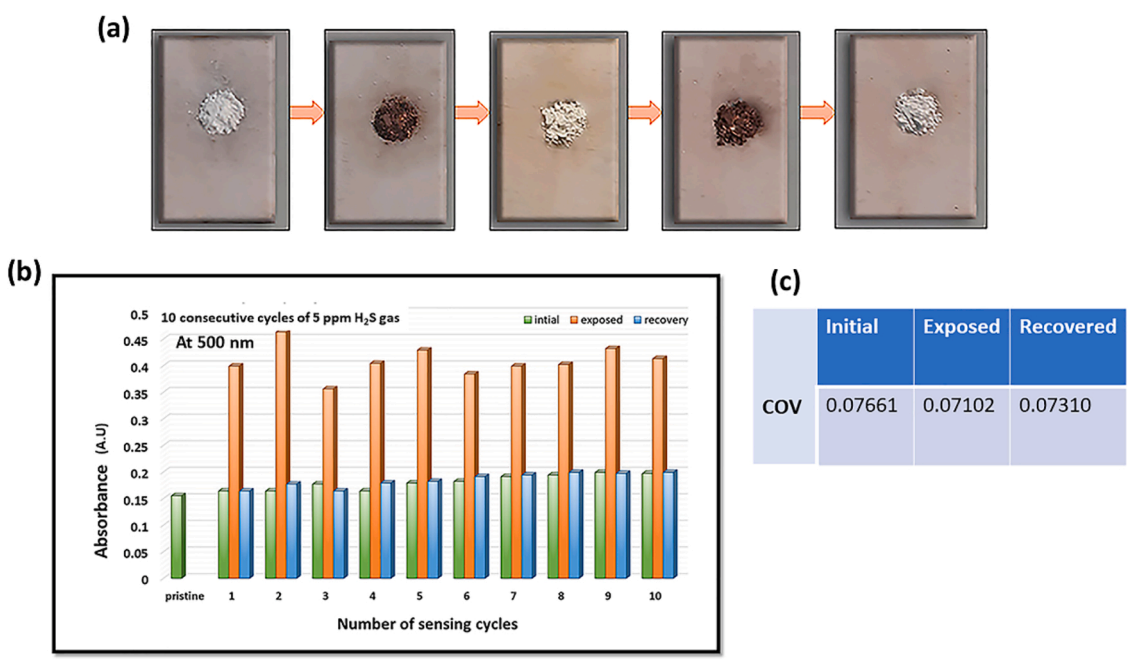

Fig. 6. (a) Optical images of two cycles (b) Absorption data in bar chart for 10 consecutive cycles and (c) Coefficient of variation, of initial, exposed and recovered Bi_2O_3 sample.

Coefficient of variation (COV) was calculated for initial, exposed and recovered samples in consecutive 20 cycles of H_2S gas. It was measured to be ~0.071 for response of sensor in 5 ppm H_2S gas. Mean value of initial (0.181) and recovered (0.184) absorbance is very close (as shown by green and blue dashed line in Fig. 6b), which supports complete recovery after multiple exposures.

Minor variations in the absorbance data after exposure and recovery are also observed. Fluctuations in sensing response during exposure may be due to the non-uniform adsorption of gas molecules on sensor surface. Absorbance of recovered sample is more than the initial in few cycles which may be due to the clearing of other atmospheric contaminations present on surface of sensor material during heating. Coefficient of variation (COV) was calculated for initial, exposed and recovered samples in consecutive 20 cycles of H_2S gas, as shown in Fig. 6(c).

4.5. Sensitivity

Bi_2O_3 nanorods were exposed to different concentration of H_2S gas from 1 to 50 ppm for 10 s at room temperature (26 ℃). Optical images were captured, and absorbance was recorded in the visible range of

wavelength from 400 to 800 nm. Fig. 7(a), shows the response of sensor material after exposing to H_2S gas in 1, 3, 5, 10, 20 and 50 ppm concentrations. Change in colour (ΔE) in Fig. 7(b) shows an increase in response of sensor towards increasing amount of gas. This experiment was repeated five times and average values are presented. Absorbance of exposed sensor material are shown in Fig. 7(c). It was observed that at 500 nm wavelength, absorbance increased uniformly with increase in the concentration of H_2S gas. Since the absorbance at 1 ppm is still higher than the pristine Bi_2O_3 so it can ascertain that material is capable of detecting low concentration of H_2S gas (lower than 1 ppm).

Absorbance values of sensor sample before and after exposure, at 500 nm was plotted in Fig. 8(a) against increasing concentrations of H_2S gas. Fig. 8(a) shows that the response of sensor towards increasing concentration of H_2S gas fits in polynomial curve. Limit of detection (LOD) was calculated to be ~310 ppb using 3-sigma method [39].

In order to find out the sensor response for higher gas concentration, sensor pellet was exposed to 70 ppm of H_2S gas for 1 min and kept on heating for recovery. However, exposed sample was not recovered even after heating for 3 min and 5 min. Absorbance plot for incomplete recovery is given in Fig.S4 in supplementary file. Full recovery was only observed after increasing heating time to 10 min, as shown in Fig. 8(b). When concentration of H_2S gas exposure to the pellet was increased to 90 ppm and recovery of sensor pellet was happened only after heating for 12 min at 300 ℃ (Fig. 8(c)). As the Bi_2O_3 nanorods were exposed to higher concentration of 100 ppm H_2S gas for 60 s, recovery was not observed after heating at 300 ℃ for more than 15 min Fig. 8(d) shows UV-Vis spectrograph of initial, exposed sensor (100 ppm) and unrecovered sensor material XRD plot of saturated Bi_2O_3 nanorods with 100 ppm H_2S exposure, (Fig. 8(e)) shows intense peaks {(310), (211), (221)} of Bi_2S_3, with an inset image of saturated sensor material powder.

4.6. Selectivity in air

Sensor pellet was exposed to 50 ppm of interfering gases i.e., NH_3, NO_2, CO_2, SO_2, C_2H_6S, $C_2H_6S_2$ and H_2S at 26 ℃. Further, a high humidity environment was created inside sealed chamber to attain 80% RH and pellet of sensor material was kept inside the chamber for 1 h. After each treatment no change in colour of pallet was observed though naked eye except H_2S. For more understanding, the absorbance spectra from 400 nm to 800 nm using UV–visible spectroscopy for each treatment was recorded and studied in comparison to pristine pellet shown in Fig. 9(a). Fig. 9(b) shows comparison of absorbance values at 500 nm of pristine sensor pellet with, exposed to gases and humidity). An increase of 2.5%, 1.9% and 1.2% in absorbance was observed during exposure to NH_3, NO_2 and SO_2 gases respectively, whereas, CO_2 gas exposure does not result in any change. High humidity (80% RH) also increased the absorbance by 12.9% from pristine sensor pellet. On the other hand, exposure of H_2S gas resulted in the increase of absorbance by 332%. This shows that the material is highly selective towards H_2S gas in air.

A sensor pellet was kept at different relative humidity, i.e., 30% RH, 50% RH and 80% RH for 1 h. No change in colour of sensor material was observed in high humidity environment (shown in Fig.S5). Absorbance of the samples after each exposure was recorded using UV-Visible spectroscopy (400–800 nm wavelength) and presented in Fig. 9(c). As shown in Fig. 9(d), the absorbance at 500 nm, was increased by 2.5% and 12.9%for 50% RH and 80% respectively as compared to the 30% RH.

4.7. Sensor application in raw animal packaging

Fig. 10(a & e) shows images of sensor (stripe, pellet and powder) responding to spoilage of chicken and pork respectively in 5 days. Mean of RGB values and optical darkness ratio (ODR) of stripe, pellet and powder were taken to plot RGB v/s time of spoilage in Fig. 10(b, c, f & g), it shows the changes in RGB values and ODR of sensors placed next to chicken and pork with each day at 26 ℃. Detailed values of RGB and ODR with respect to time is given in supplementary file (Fig.S6).

As seen in figure, chicken sample showed RGB and ODR response in less than 24 h. On the other hand, slight changes in pork sample were observed only after 48 h visible significant change was observed after 60 h.

Sensor colour in chicken sample changed to dark brown in 48 h and reached a saturation after 72 h. Sensor material having chicken sample reached saturation may be due to combination of various vapours along with H_2S gas. So, it was not able to recover on heating at 300 ℃, shown in Fig. 10(d). Pellet and powder (since stripe is of fabric, could not heat for recovery) of sensor material from pork sample was taken out after 96 h of experiment and heated at 300 ℃ for 3 min. Images of exposed

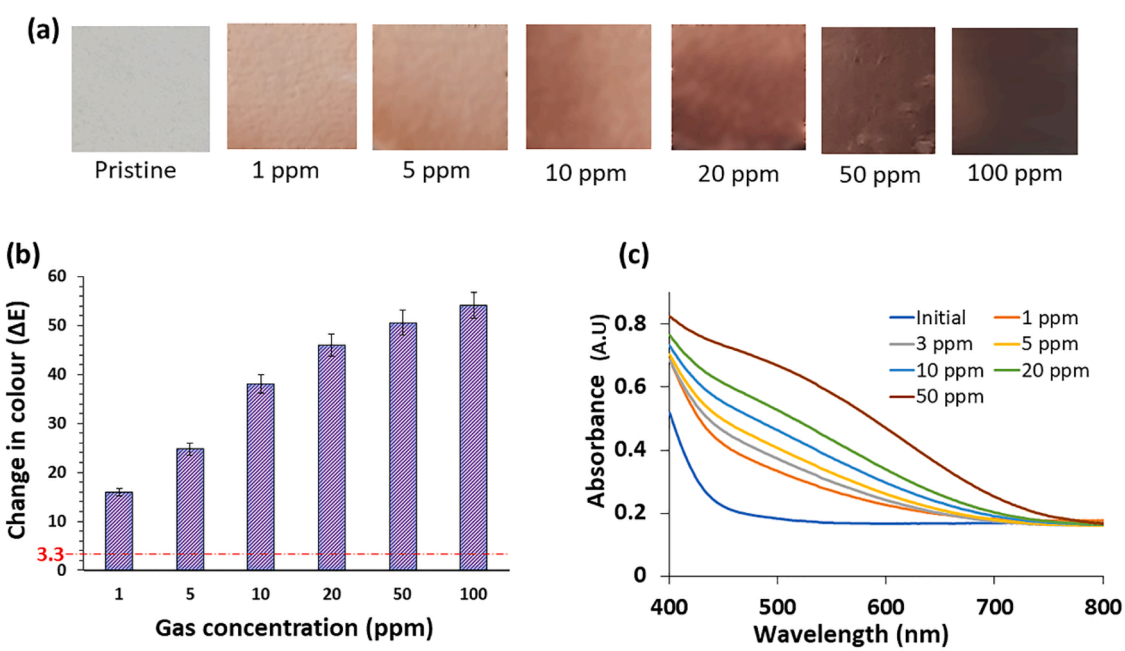

Fig. 7. Sensitivity of sensor in (a) optical images, (b) change in colour of Bi_2O ΔE ($_3$ v/s H_2S gas concentration, ΔE > 3.3 is eye-readable standard (c) UV-Vis absorbance of sensor with increasing concentration.

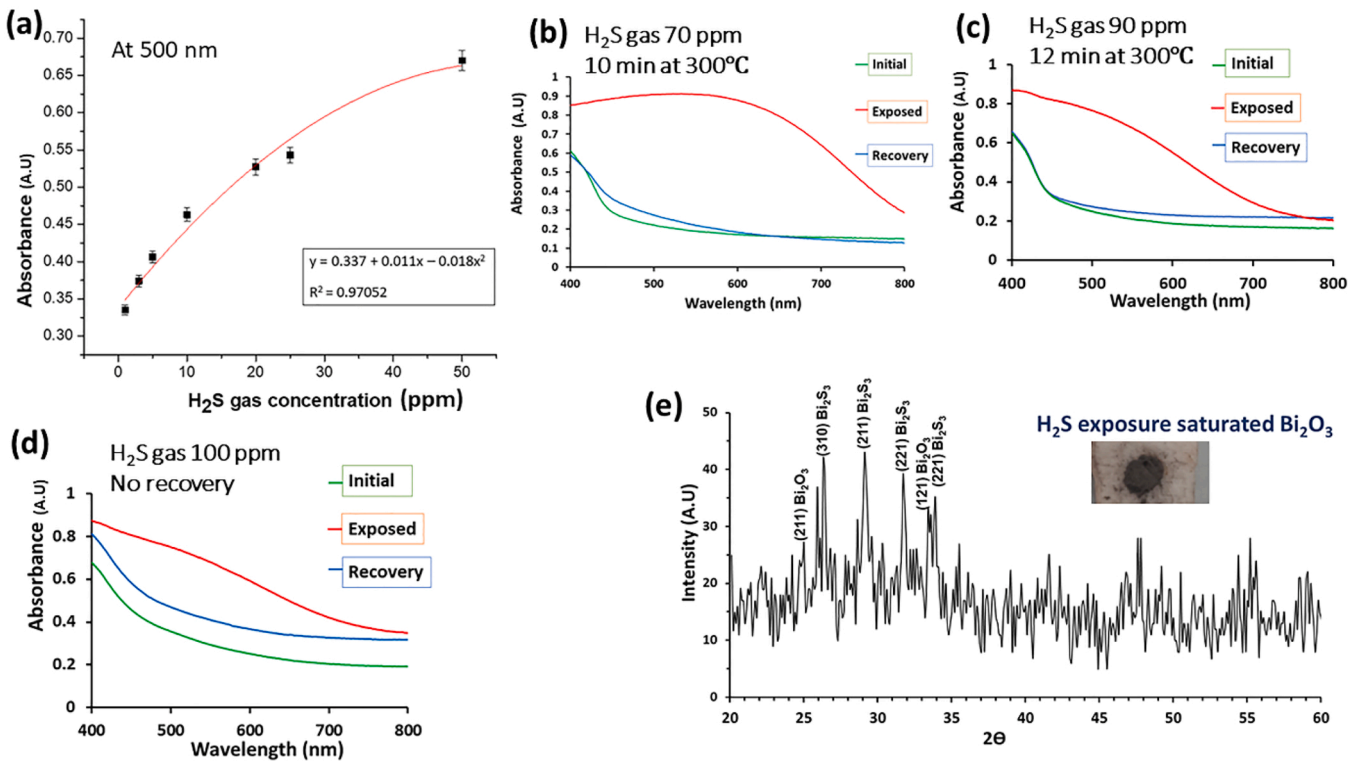

Fig. 8. (a) Absorbance at 500 nm with increasing H_2S gas concentration, absorbance spectra for sample after gas exposure of (b) 70 ppm and recovery after heating at 300 C for 10 min (c) 90 ppm and recovery after heating 300 for 12 min (d)100 ppm and no recovery after heating at 300 C for 15 min(e) XRD pattern of H_2S gas saturated Bi_2O_3 nanorods by formation of Bi_2S_3 with inset image of saturated Bi_2O_3 nanorods powder.

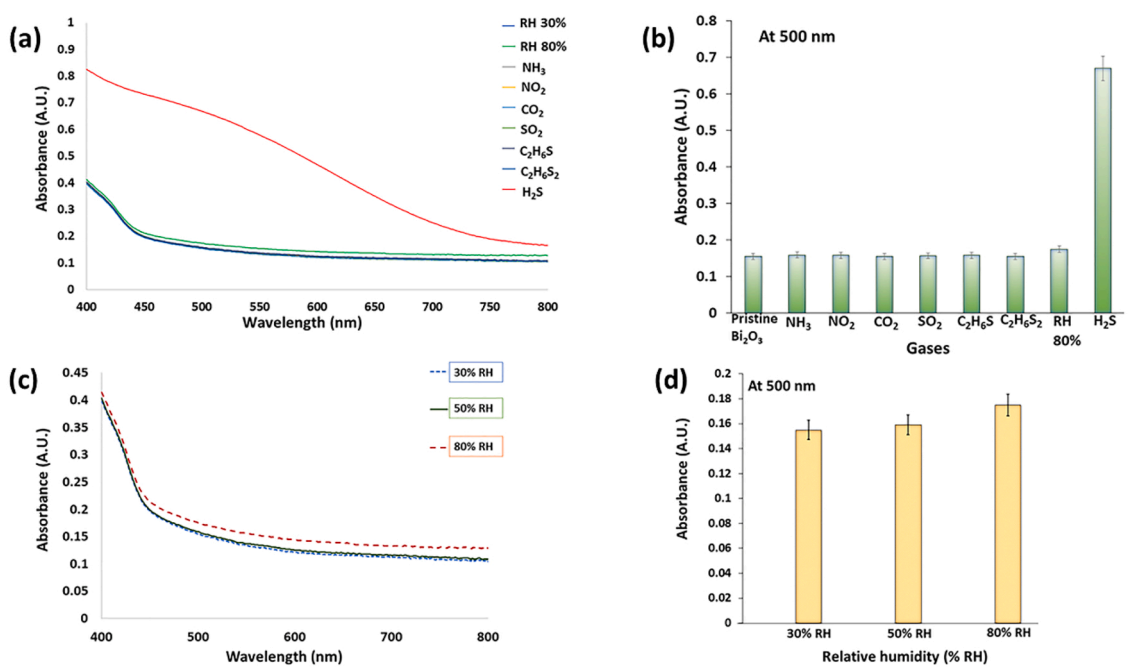

Fig. 9. (a) Absorbance of sensor towards gases and humidity in air at 26 °C (b) bar chart of absorbance of sample for different gases at 500 nm. (c) (c) Absorbance of sensor towards increasing humidity at 26 °C in the range of 400–800 nm wavelenght and (d) bar chart of absorbance of sample at different humidities at 500 nm.

sensor and recovered sensor pellet and powder are shown in Fig. 10(h). Sensor was also tested at lower degree temperature (4 °C) for chicken and fish. Visible change in colour of sensor was observed after 2 days in fish and 4 days in chicken sample, as shown in Fig. 11(a &b).

4.8. Selectivity of sensors with volatile organic compounds (VOCs)

It is reported that on meat spoilage approximately 48–50 other VOCs liberates along with H_2S gas [11], although H_2S is one of the basic gases to detect spoilage in food [40]. In order to check selectivity towards H_2S gas, sensor was exposed to 15 VOCs (Fig. 12(a)) and colour change was

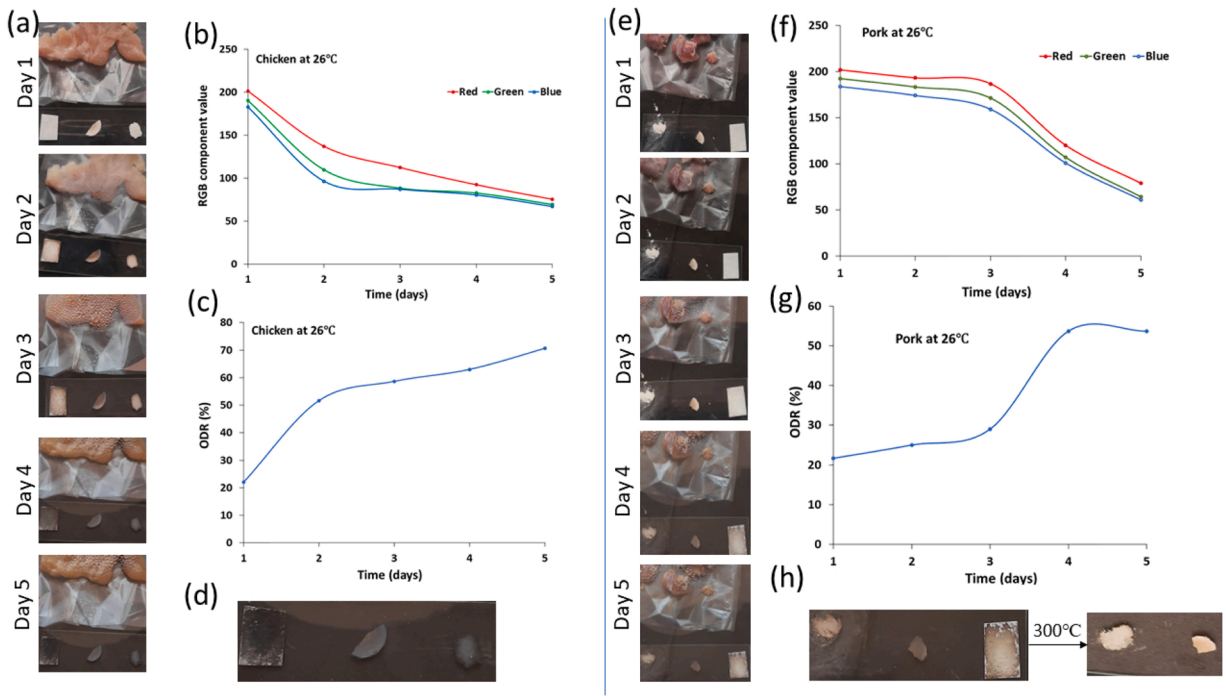

Fig. 10. Changes in meat samples with time at 26 ℃ with corresponding RGB and ODR values (a) Chicken (b) Pork.

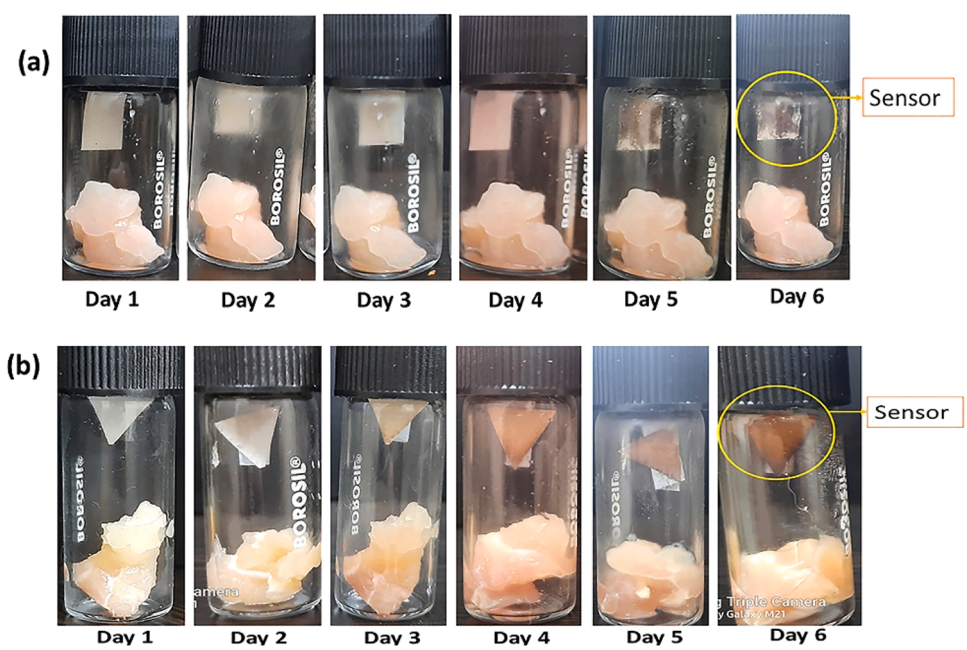

Fig. 11. Colour changes at 4 °C for 6 days in (a) Fish sample (b) Chicken sample.

observed only in presence of H_2S gas.

These results support the application of bismuth oxide nanorods in H_2S sensor for meat packaging. Sensor was tested for meat samples kept at 4 ℃ for 7 days, the results are shown in supplementary file. Which shows sensor material is capable to sense H_2S gas at lower temperatures and applicable in practical application.

5. Performance comparison

Table 1 compares various other H_2S gas sensor based on bismuth derivatives and other colorimetric sensors with our current work.

It can be observed from Table 1, that all the listed sensors with colorimetric transduction method are irreversible. However, resistive sensors based on $NaBi(MoO_4)_2$ nanoplates and Ag doped $BiFeO_3$ are reversible and quick but their higher operating temperature limits their usability. Whereas, our as fabricated sensor is pristine material with quick recovery. It is highly sensitive to H_2S gas and cost effective.

6. Proposed mechanism

Tauc plot study was performed from the absorbance spectra in Fig. 13(a). and the calculated energy bandgap vs H_2S concentration is

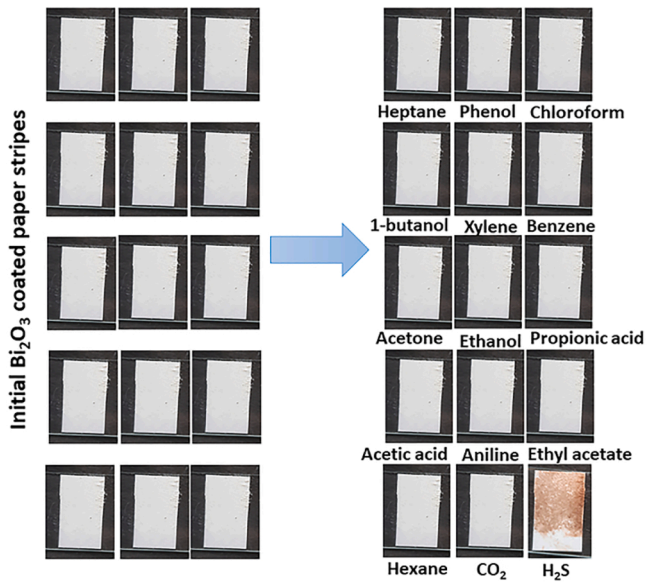

Fig. 12. Colour changes in sensor materials towards heptane, phenol, chloroform, 1-butanol, xylene, benzene, acetone, ethanol, propionic acid, acetic acid, aniline, ethyl acetate and hexane vapour and CO_2 and H_2S gas.

Table 1
Comparison with other bismuth-based sensors and other materials colorimetric sensors for H_2S gas.

Sensor material	Transduction methods/ gas concentration	Response / recovery time/ operating temp.	Ref.
Alkaline $Bi(OH)_3$	Optical / 30ppb	Quick / No recovery / 25 ℃	[18]
NaBi $(MoO_4)_2$ nanoplates	Resistive/ 5 ppm	11 s/ 4 s/ 370 ℃	[41]
Porous $BiVO_4$ thin films	Resistive/ 3 ppm	35 s/ 75 s/ 75 ℃	[42]
Ag doped $BiFeO_3$	Resistive/ 1 ppm	3 s/ 312 s/ 350 ℃	[43]
Gellan-gum and Ag NP	Colorimetric/ 0.81 M	• –/ No recovery	[11]
BCNCs–Ag NPs/ alginate–MoO_3 NPs hybrid nanocomposite	Colorimetric/ 3.27 ppm	20 min/ No recovery	[44]
2,4-dinitroben-zenesulfonyl group modified with hydrophilic PEG chain	Colorimetric/ 25 ppm	2 min/ No recovery	[45]
Orange-I, Ru nanoparticles (Ru-NPs)	Colorimetric/ 15.6Nm	5 min/ No recovery	[12]
Lead (II) acetate $[Pb(Ac)_2]$	Colorimetric/ 1 ppm	60 s/ No recovery	[15]
Lead acetate functionalised yarn	Colorimetric / 1 ppm	60 s / no recovery	[46]
Au / AgI nanoparticles	Colorimetric/ 500 ppb	30 min/ No recovery	[17]
Copper (II) complex of the azo dye 1-(2-pyridylazo)– 2-naphtol	Colorimetric / 4 ppm	2 min/ No recovery	[47]
Copper (II) chloride/ H-PAN	Colorimetric/ 8 ppm	20 min/ No recovery	[48]
Pani on cotton fabric	Colorimetric/ 1 ppm	• / No recovery	[14]
Silver-Modified Silica Sulfonic Acid (Ag-SSA)	Colorimetric/ 6.5 ppm	- /- /-	[49]
Porphyrinbased Porous Organic Polymer, $FePPOP_{epa}$	Colorimetric/ 0.1 μM	3 min/- /-	[50]
Dinitro-functionalized zr (iv)-based metal-organic framework	Colorimetric/ 20 μM	55 min/ –	[51]
Bismuth oxide nanorods	**Colorimetric / 410ppb**	**20 s/ 3 min at 300 ℃**	**Present study**

shown in Fig13(b).

As shown in Fig. 13(b), pristine sensor material has a bandgap of 2.75 eV. This bandgap is decreased with the increase in the concentration of H_2S gas. The fall in bandgap is steep up to 3 ppm gas exposure, thereafter, it slows down. This reduction in band gas is related to the formation Bi_2S_3 in the material. When material was exposed to > 100 ppm H_2S gas, the band gap was reduced to 1.34 eV and sensor became unrecoverable.

Fig. 14 Summarizes the mechanism of H_2S gas sensing by Bi_2O_3 nanorods. When synthesized Bi_2O_3 nanorods was exposed to H_2S gas, colour was changed from white to brown due to the following reaction, [52].

$$Bi_2O_3 + 3\ H_2S\ Bi_2S_3 + 3\ H_2O \quad (1)$$

Here, sulphur replaces oxygen atoms from Bi_2O_3 and conversion accompanied by the significant visible change in colour i.e from white to brown. Bismuth sulphide can be recovered bismuth oxide on oxidation. As reported by Johnson et al., Bi_2S_3 converts in to complete Bi_2O_3 at 800 ℃. During recovery Bi_2S_3 reacts with O_2 and converts into Bi_2O_3 and SO_2 [53]. Increased temperature gives energy to atoms to get agitated and grab atmospheric oxygen on the surface to oxidise itself.

$$Bi_2S_3 + O_2\ Bi_2O_3 + SO_2 \quad (2)$$

But Bi_2S_3 nanorods in the present study converted to Bi_2O_3 at 300 ℃ in three minutes during recovery. Reason of lower temperature oxidation may be due to presence of pores in structure of the sensing material, which may be responsible for enhancing oxidation rate at lower temperature. BET analysis of Bi_2O_3 nanorods shows surface area of 2.97 m^2/g, with an average pore radius of 257 nm.

It was observed that Bi_2O_3 nanorods exposed to low concentration of H_2S consists of Bi_2S_3 with bismuth oxide. Co-existence can be explained by the fact that at low concentrations of gas, the exposure is restricted to the top surface of the material. It is also supported by bandgap of bismuth oxide which reduced gradually with the increase in the H_2S gas concentration. At 50 ppm, bandgap of the sensor material approaches 1.9 eV, which is higher to the bandgap of bismuth sulfide nanorods (1.67 eV) [55–57]. This shows that Bi_2O_3 is remaining in the nanorods and Bi_2S_3 is formed at surface. Therefore, recovery is easily achieved at 300 ℃ in 3 min due to the involvement of surface reaction between Bi_2S_3 and atmospheric oxygen. However, at higher concentration (~100 ppm), H_2S gas diffuses in the subsequent layers and convert Bi_2O_3 to Bi_2S_3. Bandgap of saturated Bi_2O_3 (1.34 eV) is in accordance with bandgap of bulk Bi_2S_3 (1.34 eV) [45]. This makes the recovery difficult at 300 ℃.

When this saturated sensor material was heated at higher temperature (<300 °C) for longer duration the sensor material recovered which may be because of diffusion of atmospheric oxygen inside the sensor material and replaces sulfur from Bi_2S_3 and release SO_2. SO_2 liberation from the inside the material causes the slight damages which is evident in SEM study shown in Fig. 3(a).

7. Conclusion

A reversible, sensitive and selective H_2S gas sensor is fabricated using bismuth oxide nanorods using synthesized using green method. Nanorods turns from white to brown in presence of H_2S gas environment at room temperature of 26 ℃. Recovery of exposed materials is performed by heating at 300 ℃ for 180 s when exposed to 1–50 ppm of H_2S. Reversibility of sensor material makes it cost effective. This colorimetric sensor was successfully tested for the quality of raw animal products packaging like pork chicken and fish with time. It can be used in testing quality of other high protein foods like dairy products, eggs and wool aging prediction. Emission of H_2S gas from sewer drainage can also be easily detected using flexible sensor.

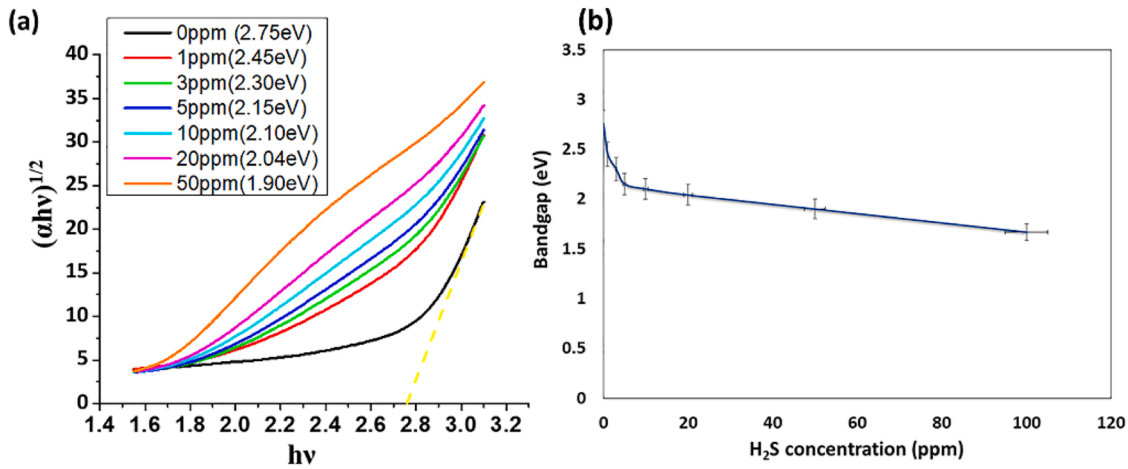

Fig. 13. (a) Tauc plot of sensor (b) plot of bandgap values v/s H_2S gas concentration.

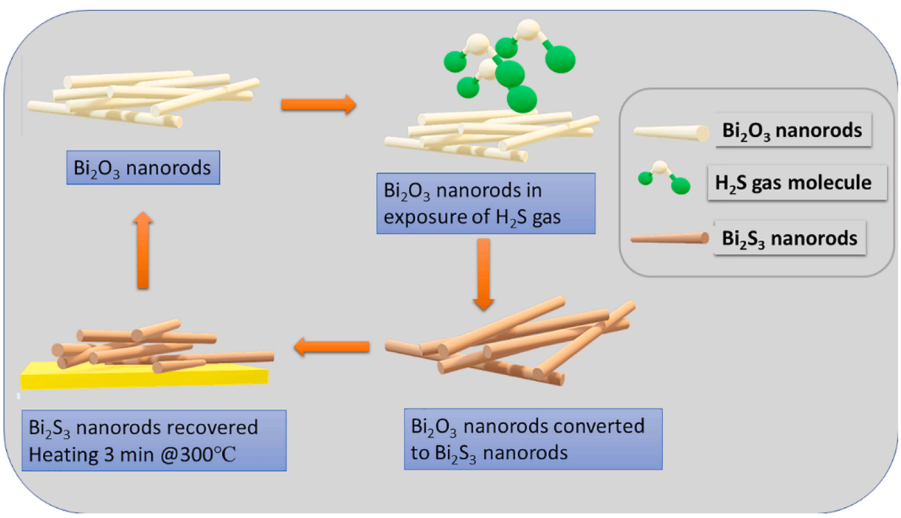

Fig. 14. Schematic diagram of sensing mechanism of sensor material.

CRediT authorship contribution statement

Monica Jaiswal: All the experimentation, result analysis and organization, Robin Kumar: result analysis, manuscript writing, organizing, communication, Ravi Mani Tripathi: Material synthesis, Ranu Nayak: Optical characterization and analysis, Jagjiwan Mittal: Characterization and analysis, Sumit Choudhary: Characterization and analysis, Satinder K Sharma: Characterization and analysis.

Declaration of Competing Interest

The authors declare the following financial interests/personal relationships which may be considered as potential competing interests: Dr. Robin Kumar reports financial support was provided by SERB DST India. Dr. Robin Kumar reports a relationship with SERB- DST India that includes: funding grants. Dr.Robin Kumar has patent pending to Amity University India.

Data Availability

Data will be made available on request.

Acknowledgment

Support of this study by the SERB, India via Grant TAR/2021/000407 is gratefully acknowledged. We are grateful to SSPL, DRDO (Delhi) and C4FED, IIT, Mandi, India for support in characterisation.

Appendix A. Supporting information

Supplementary data associated with this article can be found in the online version at doi:10.1016/j.snb.2023.133395.

References

[1] L. Chénard, S.P. Lemay, C. Laguë, Hydrogen sulfide assessment in shallow–pit swine housing and outside manure storage, J. Agric. Saf. Health 9 (2003) 285–302, https://doi.org/10.13031/2013.15458.

[2] G. Huang, E. He, Z. Wang, H. Fan, J. Shangguan, E. Croiset, Z. Chen, Synthesis and characterization of γ-Fe $_2$ O $_3$ for H $_2$ S removal at low temperature, Ind. Eng. Chem. Res. 54 (2015) 8469–8478, https://doi.org/10.1021/acs.iecr.5b01398.

[3] C. Liu, R. Zhang, S. Wei, J. Wang, Y. Liu, M. Li, R. Liu, Selective removal of H 2 S from biogas using a regenerable hybrid TiO 2 /zeolite composite, Fuel 157 (2015) 183–190, https://doi.org/10.1016/j.fuel.2015.05.003.

[4] K.-H. Kim, E.-C. Jeon, Y.-J. Choi, Y.-S. Koo, The emission characteristics and the related malodor intensities of gaseous reduced sulfur compounds (RSC) in a large industrial complex, Atmos. Environ. 40 (2006) 4478–4490, https://doi.org/10.1016/j.atmosenv.2006.04.026.

[5] Govt., OSHA, (n.d.). https://www.osha.gov/hydrogen-sulfide (accessed April 25, 2022).

[6] F.I.M. Ali, F. Awwad, Y.E. Greish, S.T. Mahmoud, Hydrogen sulfide (H 2 S) gas sensor: a review, IEEE Sens. J. 19 (2019) 2394–2407, https://doi.org/10.1109/JSEN.2018.2886131.

[7] L. Sui, T. Yu, D. Zhao, X. Cheng, X. Zhang, P. Wang, Y. Xu, S. Gao, H. Zhao, Y. Gao, L. Huo, In situ deposited hierarchical CuO/NiO nanowall arrays film sensor with enhanced gas sensing performance to H2S, J. Hazard. Mater. 385 (2020), 121570, https://doi.org/10.1016/J.JHAZMAT.2019.121570.

[8] S.K. Pandey, K.-H. Kim, K.-T. Tang, A review of sensor-based methods for monitoring hydrogen sulfide, TrAC Trends Anal. Chem. 32 (2012) 87–99, https://doi.org/10.1016/j.trac.2011.08.008.

[9] J. Zheng, H.L. Noh, H.W. Chun, B.M. Oh, J. Lee, S.K. Choi, E. Kim, D. Jung, W. S. Lee, J.H. Kim, Highly sensitive, selective, and rapid response colorimetric chemosensor for naked eye detection of hydrogen sulfide gas under versatile conditions: Solution, thin-film, and wearable fabric, Sens. Actuators B Chem. 341 (2021), https://doi.org/10.1016/j.snb.2021.130013.

[10] J. Koskela, J. Sarfraz, P. Ihalainen, A. Määttänen, P. Pulkkinen, H. Tenhu, T. Nieminen, A. Kilpelä, J. Peltonen, Monitoring the quality of raw poultry by detecting hydrogen sulfide with printed sensors, Sens. Actuators B Chem. 218 (2015) 89–96, https://doi.org/10.1016/j.snb.2015.04.093.

[11] X. Zhai, Z. Li, J. Shi, X. Huang, Z. Sun, D. Zhang, X. Zou, Y. Sun, J. Zhang, M. Holmes, Y. Gong, M. Povey, S. Wang, A colorimetric hydrogen sulfide sensor based on gellan gum-silver nanoparticles bionanocomposite for monitoring of meat spoilage in intelligent packaging, Food Chem. 290 (2019) 135–143, https://doi.org/10.1016/j.foodchem.2019.03.138.

[12] H. Li, W. Geng, X. Sun, W. Wei, X. Mu, W. Ahmad, M.M. Hassan, Q. Ouyang, Q. Chen, Fabricating a nano-bionic sensor for rapid detection of H2S during pork spoilage using Ru NPs modulated catalytic hydrogenation conversion, Meat Sci. 177 (2021), https://doi.org/10.1016/j.meatsci.2021.108507.

[13] A. Ryspayeva, T.D.A. Jones, P.A. Hughes, M.N. Esfahani, M.P. Shuttleworth, R.A. Harris, R.W. Kay, M.P.Y. Desmulliez, J. Marques-Hueso, PEI/Ag as an Optical Gas Nano-Sensor for Intelligent Food Packaging, in: 2018 IEEE 18th International Conference on Nanotechnology (IEEE-NANO), IEEE, 2018: pp. 1–4. https://doi.org/10.1109/NANO.2018.8626269.

[14] T.M. de Almeida, F. da Silveira Maranhão, F.V. de Carvalho, A. Middea, J.R. de Araujo, F.G. de Souza Júnior, H2S sensing material based on cotton fabrics modified with polyaniline, Macromol. Symp. 381 (2018), https://doi.org/10.1002/masy.201800111.

[15] J.H. Cha, D.H. Kim, S.J. Choi, W.T. Koo, I.D. Kim, Sub-parts-per-million hydrogen sulfide colorimetric sensor: lead acetate anchored nanofibers toward halitosis diagnosis, Anal. Chem. 90 (2018) 8769–8775, https://doi.org/10.1021/acs.analchem.8b01273.

[16] J. Sarfraz, A. Fogde, P. Ihalainen, J. Peltonen, The performance of inkjet-printed copper acetate based hydrogen sulfide gas sensor on a flexible plastic substrate - varying ink composition and print density, Appl. Surf. Sci. 445 (2018) 89–96, https://doi.org/10.1016/j.apsusc.2018.03.142.

[17] J. Zeng, M. Li, A. Liu, F. Feng, T. Zeng, W. Duan, M. Li, M. Gong, C.Y. Wen, Y. Yin, Au/AgI dimeric nanoparticles for highly selective and sensitive colorimetric detection of hydrogen sulfide, Adv. Funct. Mater. 28 (2018), https://doi.org/10.1002/adfm.201800515.

[18] S.M. Rosolina, T.S. Carpenter, Z.L. Xue, Bismuth-based, disposable sensor for the detection of hydrogen sulfide gas, Anal. Chem. 88 (2016) 1553–1558, https://doi.org/10.1021/acs.analchem.5b04489.

[19] F. Zhang, M. Zheng, X. Zhang, X. Cheng, M. Li, L. Huo, X. Zhou, Y. Xu, Rapid detection of H2S gas driven by the catalysis of flower-like α-Bi2Mo3O12 and its visual performance: a combined experimental and theoretical study, J. Hazard. Mater. 424 (2022), 127734, https://doi.org/10.1016/J.JHAZMAT.2021.127734.

[20] C. Milena, B. Hincapié, M. Jonathan, P. Cárdenas, J. Edgar, A. Orjuela, E.R. Parra, J. Jairo, O. Florez, PHYSICAL-CHEMICAL PROPERTIES OF BISMUTH AND BISMUTH OXIDES Synth., Charact. Appl. PROPIEDADES FÍSICO-QUÍMICAS DEL BISMUTO Y OXIDOS DE BISMUTO: Síntesis, CARACTERIZACIÓN Y APLICACIONES 79 2012 139 148.

[21] P. v Shinde, B.G. Ghule, S.F. Shaikh, N.M. Shinde, S.S. Sangale, V. v Jadhav, S. Y. Yoon, K.H. Kim, R.S. Mane, Microwave-assisted hierarchical bismuth oxide worm-like nanostructured films as room-temperature hydrogen gas sensors, J. Alloy. Compd. 802 (2019) 244–251, https://doi.org/10.1016/j.jallcom.2019.06.182.

[22] X. Gou, R. Li, G. Wang, Z. Chen, D. Wexler, Room-temperature solution synthesis of Bi2O3 nanowires for gas sensing application, Nanotechnology 20 (2009), https://doi.org/10.1088/0957-4484/20/49/495501.

[23] P. v Shinde, N.M. Shinde, S.F. Shaikh, D. Lee, J.M. Yun, L.J. Woo, A.M. Al-Enizi, R. S. Mane, K.H. Kim, Room-temperature synthesis and CO_2-gas sensitivity of bismuth oxide nanosensors, RSC Adv. 10 (2020) 17217–17227, https://doi.org/10.1039/d0ra00801j.

[24] S.S. Bhande, R.S. Mane, A. v Ghule, S.H. Han, A bismuth oxide nanoplate-based carbon dioxide gas sensor, Scr. Mater. 65 (2011) 1081–1084, https://doi.org/10.1016/j.scriptamat.2011.09.022.

[25] M. Manjula, B. Karthikeyan, D. Sastikumar, Sensing characteristics of nanocrystalline bismuth oxide clad-modified fiber optic gas sensor, Opt. Lasers Eng. 95 (2017) 78–82, https://doi.org/10.1016/j.optlaseng.2017.04.003.

[26] Y. Zhao, Y. Xie, X. Zhu, S. Yan, S. Wang, Surfactant-free synthesis of hyperbranched monoclinic bismuth vanadate and its applications in photocatalysis, gas sensing, and lithium-ion batteries, Chem. Eur. J. 14 (2008) 1601–1606, https://doi.org/10.1002/chem.200701053.

[27] R.P. Rao, S. Mishra, R.M. Tripathi, S.K. Jain, Bismuth oxide nanorods: phytochemical mediated one-pot synthesis and growth mechanism, Inorg. Nano-Met. Chem. (2021) 1–8, https://doi.org/10.1080/24701556.2021.1980037.

[28] A. Kaur, B. v Kranthi, ISSN: 2249–0868 Foundation of Computer Science FCS, 2012. ⟨www.ijais.org⟩.

[29] P. Chaudhary, Anand K. Chaudhari, A.N. Cheeran, Sharda Godara, Color transform based approach for disease spot detection on plant leaf, Int. J. Comput. Sci. Telecommun. 3 (2012) 65–70.

[30] A. Vichi, M. Ferrari, C.L. Davidson, Color and opacity variations in three different resin-based composite products after water aging, Dent. Mater. 20 (2004) 530–534, https://doi.org/10.1016/J.DENTAL.2002.11.001.

[31] J.F. M. J, N. C. V, S. S, α-Bi $_2$ O $_3$ photoanode in DSSC and study of the electrode–electrolyte interface, RSC Adv. 5 (2015) 78299–78305. https://doi.org/10.1039/C5RA12760B.

[32] A.K. Dutta, S.K. Maji, K. Mitra, A. Sarkar, N. Saha, A.B. Ghosh, B. Adhikary, Single source precursor approach to the synthesis of Bi2S3 nanoparticles: a new amperometric hydrogen peroxide biosensor, Sens. Actuators B Chem. 192 (2014) 578–585, https://doi.org/10.1016/j.snb.2013.11.030.

[33] L. Kumari, J.H. Lin, Y.R. Ma, Laser oxidation and wide-band photoluminescence of thermal evaporated bismuth thin films, J. Phys. D. Appl. Phys. 41 (2008), https://doi.org/10.1088/0022-3727/41/2/025405.

[34] F.D. Hardcastle, I.E. Wachs, The Molecular Structure of Bismuth Oxide by Raman Spectroscopy, n.d.

[35] K. Trentelman, A note on the characterization of bismuth black by Raman microspectroscopy, J. Raman Spectrosc. 40 (2009) 585–589, https://doi.org/10.1002/jrs.2184.

[36] P. Devendran, T. Alagesan, K. Pandian, Synthesis and characterization of Bi2S3 nanorods decorated on carbon sphere and study its electrochemical application, Adv. Mater. Res. 938 (2014) 215–220, https://doi.org/10.4028/WWW.SCIENTIFIC.NET/AMR.938.215.

[37] X. Yu, C. Cao, Photoresponse and field-emission properties of bismuth sulfide nanoflowers, Cryst. Growth Des. 8 (2008) 3951–3955, https://doi.org/10.1021/cg701001m.

[38] I. Zumeta-Dubé, J.L. Ortiz-Quiñonez, D. Díaz, C. Trallero-Giner, V.F. Ruiz-Ruiz, First order raman scattering in bulk Bi2S3 and quantum dots: Reconsidering controversial interpretations, J. Phys. Chem. C 118 (2014) 30244–30252, https://doi.org/10.1021/jp509636n.

[39] S.E. Vignaduzzo, P.M. Castellano, T.S. Kaufman, Method development and validation for the simultaneous determination of meloxicam and pridinol mesylate using RP-HPLC and its application in drug formulations, J. Pharm. Biomed. Anal. 46 (2008) 219–225, https://doi.org/10.1016/j.jpba.2007.09.011.

[40] H. Cheng, H. Xu, D. Julian McClements, L. Chen, A. Jiao, Y. Tian, M. Miao, Z. Jin, Recent advances in intelligent food packaging materials: Principles, preparation and applications, Food Chem. 375 (2022), https://doi.org/10.1016/j.foodchem.2021.131738.

[41] M. Xu, Z. Lin, Y. Hong, Z. Chen, P. Fu, D. Tang, Preparation and hydrogen sulfide gas-sensing performances of RuO2/NaBi(MoO4)2nanoplates, J. Alloy. Compd. 688 (2016) 504–509, https://doi.org/10.1016/j.jallcom.2016.07.007.

[42] C. Li, X. Qiao, J. Jian, F. Feng, H. Wang, L. Jia, Ordered porous BiVO4 based gas sensors with high selectivity and fast-response towards H2S, Chem. Eng. J. 375 (2019), https://doi.org/10.1016/j.cej.2019.121924.

[43] T. Bagwaiya, P. Khade, H.A. Reshi, S. Bhattacharya, V. Shelke, M. Kaur, A. K. Debnath, K.P. Muthe, S.C. Gadkari, in: A.I.P. Conf Proc (Ed.), Investigation on Gas Sensing Properties of Ag Doped BiFeO3, American Institute of Physics Inc, 2018, https://doi.org/10.1063/1.5028910.

[44] P. Sukhavattanakul, H. Manuspiya, Influence of hydrogen sulfide gas concentrations on LOD and LOQ of thermal spray coated hybrid-bacterial cellulose film for intelligent meat label, Carbohydr. Polym. 254 (2021), 117442, https://doi.org/10.1016/j.carbpol.2020.117442.

[45] P. Xiao, J. Liu, Z. Wang, F. Tao, L. Yang, G. Yuan, W. Sun, X. Zhang, A color turn-on fluorescent probe for real-time detection of hydrogen sulfide and identification of food spoilage, Chem. Commun. 57 (2021) 5012–5015, https://doi.org/10.1039/d1cc01369f.

[46] D.H. Kim, J.H. Cha, J.Y. Lim, J. Bae, W. Lee, K.R. Yoon, C. Kim, J.S. Jang, W. Hwang, I.D. Kim, Colorimetric dye-loaded nanofiber yarn: eye-readable and weavable gas sensing platform, ACS Nano 14 (2020) 16907–16918, https://doi.org/10.1021/acsnano.0c05916.

[47] L. Engel, I. Benito-Altamirano, K.R. Tarantik, C. Pannek, M. Dold, J.D. Prades, J. Wöllenstein, Printed sensor labels for colorimetric detection of ammonia, formaldehyde and hydrogen sulfide from the ambient air, Sens. Actuators B Chem. 330 (2021), https://doi.org/10.1016/j.snb.2020.129281.

[48] L. Engel, K.R. Tarantik, I. Benito-Altamirano, C. Pannek, J.D. Prades, J. Wollenstein, Screen-Printable Colorimetric Sensors for the Monitoring of Toxic Gases in Ambient Air, in: 2019 IEEE International Conference on Flexible and Printable Sensors and Systems (FLEPS), IEEE, 2019: pp. 1–3. https://doi.org/10.1109/FLEPS.2019.8792300.

[49] H. Wu, Q. Cheng, H. Mao, W. Zhang, L. Lin, Functionalized organic–inorganic hybrid composites used as colorimetric chemosensors for hydrogen sulfide detection, J. Appl. Polym. Sci. 139 (2022) 52312, https://doi.org/10.1002/APP.52312.

[50] Y. Li, Y. Fang, W. Gao, X. Guo, X. Zhang, Porphyrin-Based Porous Organic Polymer as Peroxidase Mimics for Sulfide-Ion Colorimetric Sensing, ACS Sustain Chem Eng. (2020) acssuschemeng.0c03045. https://doi.org/10.1021/acssuschemeng.0c03045.

[51] R. Dalapati, S.N. Balaji, V. Trivedi, L. Khamari, S. Biswas, A dinitro-functionalized Zr(IV)-based metal-organic framework as colorimetric and fluorogenic probe for highly selective detection of hydrogen sulphide, Sens. Actuators B Chem. 245 (2017) 1039–1049, https://doi.org/10.1016/j.snb.2017.02.005.

[52] B.-G. Kim, D.-W. Park, I. Kim, H.-C. Woo, Selective oxidation of hydrogen sulfide over mixture catalysts of V–Sb–O and Bi2O3, Catal. Today 87 (2003) 11–17, https://doi.org/10.1016/j.cattod.2003.10.007.
[53] V.S. Johnson, R.J. White, S.E. Dann, K. Hellgardt, Structural investigation of the high-temperature oxidation of bismuth sulfide using TPO-MS and in situ X-ray diffraction techniques, Ind. Eng. Chem. Res. 43 (2004) 3127–3132, https://doi.org/10.1021/ie049960a.
[55] Q. Han, J. Chen, X. Yang, D. Lu, X. Wang, Preparation of uniform Bi2S3 nanorods using xanthate complexes of bismuth (III), J. Phys. Chem. C 111 (2007) 14072–14077, https://doi.org/10.1021/jp0742766.
[56] M.-R. Gao, S.-H. Yu, J. Yuan, W. Zhang, M. Antonietti, Supporting Information Poly (ionic liquid)-Mediated Morphogenesis of Bismuth Sulfide with a Tunable Band Gap and Enhanced Electrocatalytic Properties, n.d.
[57] M.-R. Gao, S.-H. Yu, J. Yuan, W. Zhang, M. Antonietti, Poly(ionic liquid)-mediated morphogenesis of bismuth sulfide with a tunable band gap and enhanced electrocatalytic properties, Angew. Chem. 128 (2016) 13004–13008, https://doi.org/10.1002/ange.201607221.

Monica Jaiswal received her B.sc degree in physics from Barkatullah University, Bhopal, Madhya Pradesh (2013) and M.Sc degree In physics with material science specialisation from Christ University, Bangalore (2016). Currently pursuing Ph.D on gas sensors under Dr. Jagjiwan Mittal from Amity University, Noida, Uttar Pradesh. Her field of interest are synthesis of nanoparticles, nanocomposites, gas sensing experiments, studying sensing mechanism.

Dr. Robin Kumar received the M.Sc and M.Tech (Microelectronics & VLSI design) from the Kurukshetra University, India and recently completed his Ph.D. He is currently working as an Assistant Professor at Amity Institute of Nanotechnology, Amity University, Noida, India since 2007. His research interests are sensors and sensor technology, MEMS, device modelling.

R.M. Tripathi received his B.Sc. degree in biology in 2002 from Gorakhpur University and M.Sc degree in biotechnology from Barkatullah University in 2004. Further he enhanced his educational qualification by receiving M.Phil. degree in biotechnology from Allagapa University in 2008. He has submitted his Ph.D. thesis at Jiwaji University in 2014, Gwalior, India and working as Asst. Professor in Amity Institute of Nanotechnology, Amity University, Noida, India.

Dr Ranu Nayak has several years of post-doctoral research experience in materials science. Her expertise and research interests include, physico chemical characterization of thin film and nanomaterials, mass spectrometry for proteomic applications, electrochemical and physical deposition of metal, semiconductor nanostructures for sensing, and energy applications; development of polymer nanocomposites for environmental applications such as water purification. During her PhD she bagged awards from Govt of India in terms of fellowships. She has published several research articles in high impact journals, book chapters and also patents. She has run two Govt. funded research projects and her ongoing project from ICMR is a part of the current manuscript.

Dr. Jagjiwan Mittal received his M Tech and PhD degrees in Chemistry from IIT Delhi, India. Besides India, he worked as JSPS fellow in Japan, CNRS Associate Researcher in France, and Post doc. in Taiwan. His specialisation is in materials chemistry particularly carbon and graphitic materials including graphene and carbon nanotubes. His current research work includes development and application studies on different nanomaterials ranges from carbon nanotubes, graphene, solder metals and alloys, metal nanoparticles and nanofibers. At present, he is working as Associate professor in Amity University He can be contacted at jmittal@amity.edu.

Sumit Choudhary(Member, IEEE) received the M.Tech. degree in microelectronics and VLSI design from the Department of Electronic Science, Kurukshetra University, Kurukshetra, India, in 2012.,From 2012–2017, he was a Faculty with the Department of Electronic Science, Kurukshetra University (KU). Since 2017, he has been working as a Doctoral Research Fellow with the School of Computing and Electrical Engineering (SCEE), Indian Institute of Technology Mandi, Mandi, India. His research interests include CMOS, microelectronics, FinFET devices nanofabrication, and characterization.

Dr. Satinder K. Sharma received the M.S. degree in physics (Electronic Science) from Himachal Pradesh University, Shimla, India, in 2002, and the Ph.D. degree from the Department of Electronic Science, Kurukshetra University, Kurukshetra, India, in 2007. His Ph.D. thesis was on silicon-based gate dielectric materials for VLSI/ ULSI technology. From 2007–2010, he was a Post-Doctoral Fellow at the DST Unit on Nanosciences and Nanotechnology, Dept. CHE, Indian Institute of Technology (IIT) Kanpur, Kanpur, India. From 2010–2012, he worked as a member of faculty in the Electronics and Microelectronics Division, Indian Institute of Information Technology (IIIT), Allahabad, India. From 2012 onwards, he has been working as a professor in the School of Computing and Electrical Engineering (SCEE), Indian Institute of Technology (IIT), Mandi, (Himachal Pradesh), India. His current research interests include microelectronics circuits and system, CMOS device, fabrication and characterization, nano/microfabrication and design, polymer nanocomposite, sensors, photovoltaic, and self-assembly.